Available online at www.sciencedirect.com

ScienceDirect

Green Energy & Environment 3 (2018) 239–246

www.keaipublishing.com/gee

Research paper

Fabrication of CuO_x thin-film photocathodes by magnetron reactive sputtering for photoelectrochemical water reduction

Tian Xie [a], Tao Zheng [b], Ruiling Wang [a], Yuyu Bu [c,*], Jin-Ping Ao [a,c,*]

[a] Institute of Technology and Science, Tokushima University, 2-1 Minami-Josanjima, Tokushima 770-8506, Japan
[b] National Institute of Technology, Anan College, 265 Aoki Minobayashi, Anan, Tokushima 774-0017, Japan
[c] Key Laboratory of Wide Band-Gap Semiconductor Materials and Devices, School of Microelectronics, Xidian University, Xi'an 710071, China

Received 10 November 2017; revised 9 January 2018; accepted 11 January 2018
Available online 2 February 2018

Abstract

The CuO_x thin film photocathodes were deposited on F-doped SnO_2 (FTO) transparent conducting glasses by alternating current (AC) magnetron reactive sputtering under different Ar:O_2 ratios. The advantage of this deposited method is that it can deposit a CuO_x thin film uniformly and rapidly with large scale. From the photoelectrochemical (PEC) properties of these CuO_x photocathodes, it can be found that the CuO_x photocathode with Ar/O_2 30:7 provide a photocurrent density of -3.2 mA cm^{-2} under a bias potential -0.5 V (vs. Ag/AgCl), which was found to be twice higher than that of Ar/O_2 with 30:5. A detailed characterization on the structure, morphology and electrochemical properties of these CuO_x thin film photocathodes was carried out, and it is found that the improved PEC performance of CuO_x semiconductor photocathode with Ar/O_2 30:7 attributed to the less defects in it, indicating that this Ar/O_2 30:7 is an optimized condition for excellent CuO_x semiconductor photocathode fabrication.

Keywords: CuO_x thin film; Magnetron sputtering; Photocathode; Defect controlling

1. Introduction

Photoelectrochemical (PEC) water splitting for hydrogen evolution is a potential technique to solve the crises of energy shortage and environment pollution [1]. In recent years, this research area has achieved great progress by the persistent efforts of the researchers. Related studies indicated that the methods to improve the overall solar-to-hydrogen efficiency in PEC devices mainly include: (1) obtaining better light absorption by engineering the absorber layer morphology of semiconductors [2,3]; (2) improving charge transfer efficiency of the semiconductors by establishing microstructure or nanostructure [4,5]; (3) improving the heterogeneous reaction kinetics by attaching catalysts to the photoelectrodes surfaces [6,7]; (4) protecting the semiconductors from corrosion by building surface passivation layers [8,9]; (5) reducing the rate of electrons–holes recombination by surface state passivation [10] or surface catalyst layers [11].

Cu_2O and CuO are considered as promising photocatalytic materials for water splitting owing to their cost-effective and abundant resources [12]. Yang et al. [13] prepared a Cu_2O/CuO bilayered composite photocathode by electrodeposition and thermal oxidation methods, this photocathode achieved a 3.15 mA cm^{-2} HER photocurrent at a bias potential of 0.4 V vs. RHE. Cu_2O is a kind of p-type semiconductors, its direct bandgap is approximately 2.0 eV [14], which has a high corresponding theoretical photocurrent and a high efficiency of light converts to hydrogen [15]. Compared with these hot research visible light responsive PEC materials, such as Ta_2N_3 [16],

* Corresponding authors.
E-mail addresses: buyuyuqust@163.com (Y. Bu), jpao@ee.tokushima-u.ac.jp (J.-P. Ao).

https://doi.org/10.1016/j.gee.2018.01.003

$BiVO_4$ [17,18], WO_3 [19,20] and Fe_2O_3 [21,22], etc., Cu_2O shows better cost-performance and higher theoretical maximum PEC water splitting conversion efficiency, it is highly deemed as a potential industry applications material for PEC water splitting. And the conduction band potential of Cu_2O is much negative than the water reduction potential (as shown in Fig. 1), the photogenerated electrons can reduce water to hydrogen smoothly. However, the valence band potential of Cu_2O is just near the water oxidation potential, so that the water oxidation process is difficult to drive by this small over potential. Simultaneously, its poor stability and fast carriers recombination rate [23] also limits the photoelectrochemical performance of Cu_2O. Consider compounding Cu_2O with other semiconductors, such as CuO [24,25], which can provide a much positive valence potential and then improve the water oxidation process. CuO is another semiconductor in cupper oxides group. It is a kind of p-type semiconductor with a direct bandgap of 1.4 eV [26], so that the light response range of CuO is much larger than Cu_2O, corresponding to a higher PEC performance than that of Cu_2O in theory. In addition, CuO has strong absorption under ultraviolet [27], which widens the absorption spectra of Cu_2O [28]. Copper oxide thin film can be prepared by several methods at present, such as magnetron sputtering [29], sol-gel [12], metal organic chemical vapor deposition [30], electrochemical deposition [31]. Among these methods, magnetron sputtering is a simple and easy-to-control deposition method, which can be scaled up to mass-produced for industrial applications [32]. The thin film deposited by magnetron sputtering is uniform and the properties of the thin film can be reproducible.

In this study, we report on the PEC performance of CuO_x photoelectrodes prepared by AC magnetron reactive sputtering. The electrochemical properties of the CuO_x photoelectrodes were characterized by electrochemical impedance spectroscopy (EIS), Mott–Schottky and PEC performance measurement. Scanning electron microscope (SEM), X-ray diffraction (XRD), Raman spectrum, X-ray photoelectron spectroscope (XPS) and UV–Vis diffuse reflectance spectrum were utilized to characterize the structures and morphologies of the CuO_x thin films.

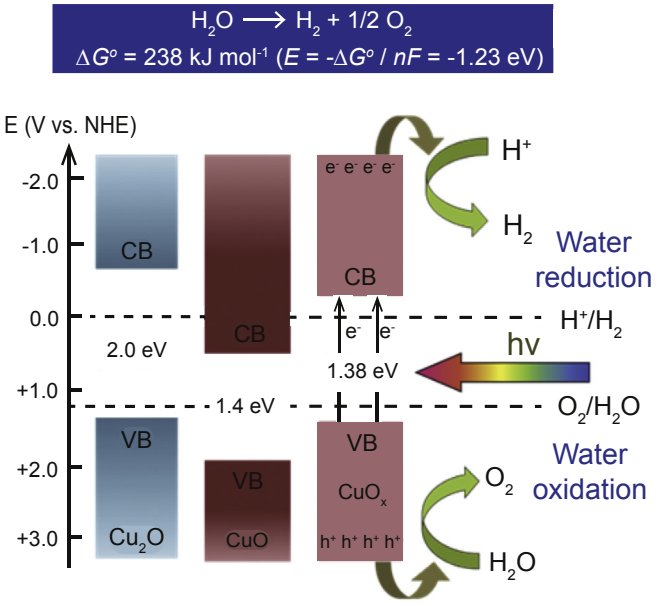

Fig. 1. Band diagram of mixed valence copper oxide system.

2. Experimental

2.1. Preparation of CuO_x thin films and photoelectrodes

FTO glasses (1.2 cm × 1.0 cm) were ultrasonically cleaned with ethanol and acetone (1:1) mixed solutions for 5 min firstly, then ultrasonically cleaned with ultrapure water for 5 min, and blow-dried with N_2. The CuO_x thin films were prepared by AC magnetron reactive sputtering at room temperature in Ar and O_2 ambient, using a target metal of copper. During the process of sputtering, the deposition chamber was pumped down to a pressure of 2×10^{-5} Pa. The target was cleaned by a pre-sputtering in Ar gas atmosphere for 5 min, then followed by a second pre-sputtering with Ar and O_2 mixture ambient for 3 min. In this experiment, the sputtering power was fixed at 30 W, and the Ar gas flow was fixed at 30 sccm. The O_2 gas flow was adjusted from 5 sccm to 9 sccm to analyze the effects of Ar/O_2 gas ratio on PEC performance of the products. The thickness of the CuO_x thin films is approximately 220 nm. After deposition, use a conductive sliver tape to connect copper wires with the conductive parts of FTO glasses. And after the conductive tape dried, isolated the exposed conductive parts of FTO glasses with parafilm.

2.2. Characterization

The microstructures of the products were characterized by X-ray diffraction (X'Pert Powder, PANalytical B.V., Almelo, The Netherlands), scanning electron microscope (JSM-6700F, JEOL, Tokyo, Japan) and Raman spectrum (STR-500, Cornes Technologies LTD., Tokyo, Japan). X-ray photoelectron spectroscopy (PHI 5000 Versa Probe, 2ULVAC-PHI, Chigasaki, Japan) was utilized to investigate the element composition, the element chemical and electronic state of the products. Whereas their light absorption capabilities were analyzed by UV–Vis diffuse reflectance spectrophotometer (U-2600, SHIMADZU Co., Kyoto, Japan).

2.3. Photoelectrochemical measurements

The Photoelectrochemical test was performed on CHI660D Electrochemical Workstation (Shanghai Chenhua Instrument Co., Ltd., Shanghai, China). In which, using a three-electrode system, the prepared CuO_x thin film (1 cm^2), Pt sheet and Ag/AgCl (saturated KCl) electrode were acted as the working electrode, counter electrode and reference electrode, respectively. The three-electrode was immersed into 0.1 mol L^{-1} Na_2SO_4 electrolyte solutions. The incident light is from 300 W Xe lamp light source (PLS-SXE300, Beijing bofeilai Technology Co., Ltd., Beijing, China) with a light intensity adjusted to 200 mW cm^{-2}. The photoinduced current with potential was tested from 0.5 V to −0.5 V (vs. Ag/AgCl) with

a scan rate of 0.02 V s^{-1}, and the photoinduced I–V curve was performed during light on and off in turns with 1 s respectively. The electrochemical impedance spectroscopy test was measured with a frequency range from 10^6 to 10^{-1} Hz, and an AC voltage magnitude of 5 mV, under dark state. Mott–Schottky plots had potential scanning range of −0.5 V to 0.5 V with a frequency of 10 Hz and an AC voltage magnitude of 10 mV.

3. Results and discussion

3.1. Crystal phase analyses

XRD patterns of the CuO_x thin films are shown in Fig. 2. The diffraction patterns for the CuO_x thin films have nine broad peaks at 30.4°, 32.5°, 36.4°, 43.2°, 46.3°, 48.7°,58.3°,74.1° and 77.3° corresponding to Cu_2O (110), CuO (110), Cu_2O (111), Cu (222), CuO (−112), CuO (−202), CuO (202), Cu (220) and Cu_2O (222), respectively. The crystal system of Cu_2O and CuO can be confirmed to be cubic and monoclinic. The XRD results show that the Cu_2O (111), CuO (−200) and Cu_2O (222) crystal planes develop on the thin film Ar/O_2 30:7, and the Cu (111) and Cu (220) crystal planes develop on the CuO_x thin films Ar/O_2 30:5 and 30:6. The CuO (110) and (202) crystal planes widely develop on the thin film Ar/O_2 30:5, due to the decrease of O_2 gas flow. The XRD results indicate that a mixture of cuprite (Cu_2O) and tenorite (CuO) was produced under different atmosphere.

Fig. 3 shows the SEM images of the top views of the CuO_x thin film photoelectrodes. Fig. 3a–e shows the morphologies of the CuO_x thin film photoelectrodes surfaces at a lower magnification. As we can see from Fig. 3a and b, the CuO_x thin films consist of low crystallinity roughly 100 nm in diameter. With the increase of Ar/O_2, the CuO_x particles grow to 150 nm in diameter, and seem to higher crystallinity, as shown in Fig. 3c–e. To study the microstructure of the CuO_x particles under high Ar/O_2 ratios, we recorded SEM images at a higher magnification. As we can see from Fig. 3f–h, it clearly shows the cubic shapes of the CuO_x particles, indicating that with the increase of Ar/O_2, the CuO_x turns to higher crystallinity, finally forms cubic shapes. According to the results, the as-deposited thin films were quite evenly distributed on the surface of the FTO glasses, and crack was not found on the thin film surfaces.

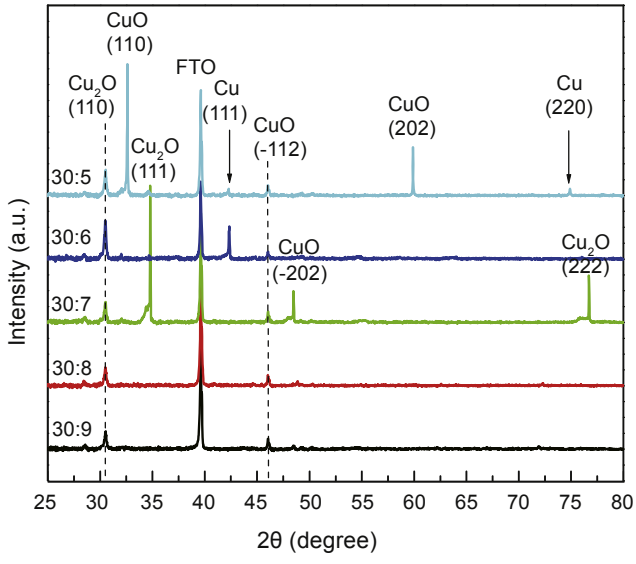

Fig. 2. XRD patterns of CuO_x composite with different Ar/O_2 ratios.

Fig. 4 shows the Raman spectra of CuO_x thin films. As we can see from the Raman spectra, a weak peak at 217 cm^{-1} and a stronger peak at 294 cm^{-1} belong to Cu_2O and CuO. It is difficult to notice the weak peak of Cu_2O at 217 cm^{-1}, demonstrating the content of CuO is higher than Cu_2O synthesized in these samples. The results of Raman spectra show that the products of sputtered thin films are Cu_2O and CuO, which are in agreement with the XRD results.

3.2. XPS and optical characterization

XPS was further used to evaluate the chemical and electronic states of CuO_x thin films. Fig. 5 shows the XPS spectra of the CuO_x composite with different Ar/O_2 ratios. As we can see from Fig. 5, there is no difference in the shape of the spectrum between these three gas ratios of the thin films. The total survey spectrum is shown in Fig. 5A, scans of the prepared where performed in a binding energy range from 0 to 1100 eV. Fig. 5B and C show the XPS spectra of Cu 2p and O 1s, where peaks at 932.9 eV and 952.8 eV represent the characteristic peaks of Cu $2p_{3/2}$ and Cu $2p_{1/2}$, indicating that Cu element existed in the form of Cu^{2+} in the compound. The strong Cu^{2+} satellite peaks at 943.7 eV and 962.2 eV indicate that the main component of these thin films is Cu^{2+}. 529.6 eV represents the O 1s characteristic peak. These results disclose that most of the products prepared by magnetron reactive sputtering are CuO, which are consistent with the results of Raman spectra.

The UV–Vis absorption spectra of CuO_x thin films are shown in Fig. 6. The absorption wavelength of the CuO_x thin films can be calculated by the intercept of the tangent and wavelength axis. According to Fig. 6d and e, the absorption wavelength is 490 nm and 590 nm, respectively, indicating that the CuO_x thin films possessed the ability to respond to visible light. However, the light absorptions of the thin films are not strong in the visible light region. Fig. 6a–c shows that the absorption wavelength is 880 nm, and the light absorptions of these thin films are very strong in the whole wavelength range. It can be seen that the optical absorption intensity of CuO_x is obviously lower with the increase of O_2 gas flow. The UV/Vis results indicate that the CuO_x thin films under lower O_2 gas flow (Ar/O_2 = 30:5, 30:6, 30:7) have strong light absorption capability in the whole wavelength range (ultraviolet and visible light region).

3.3. Photoelectrochemical property

EIS can be utilized to characterize the interface charges transfer rate and the degree of interfacial electron reaction,

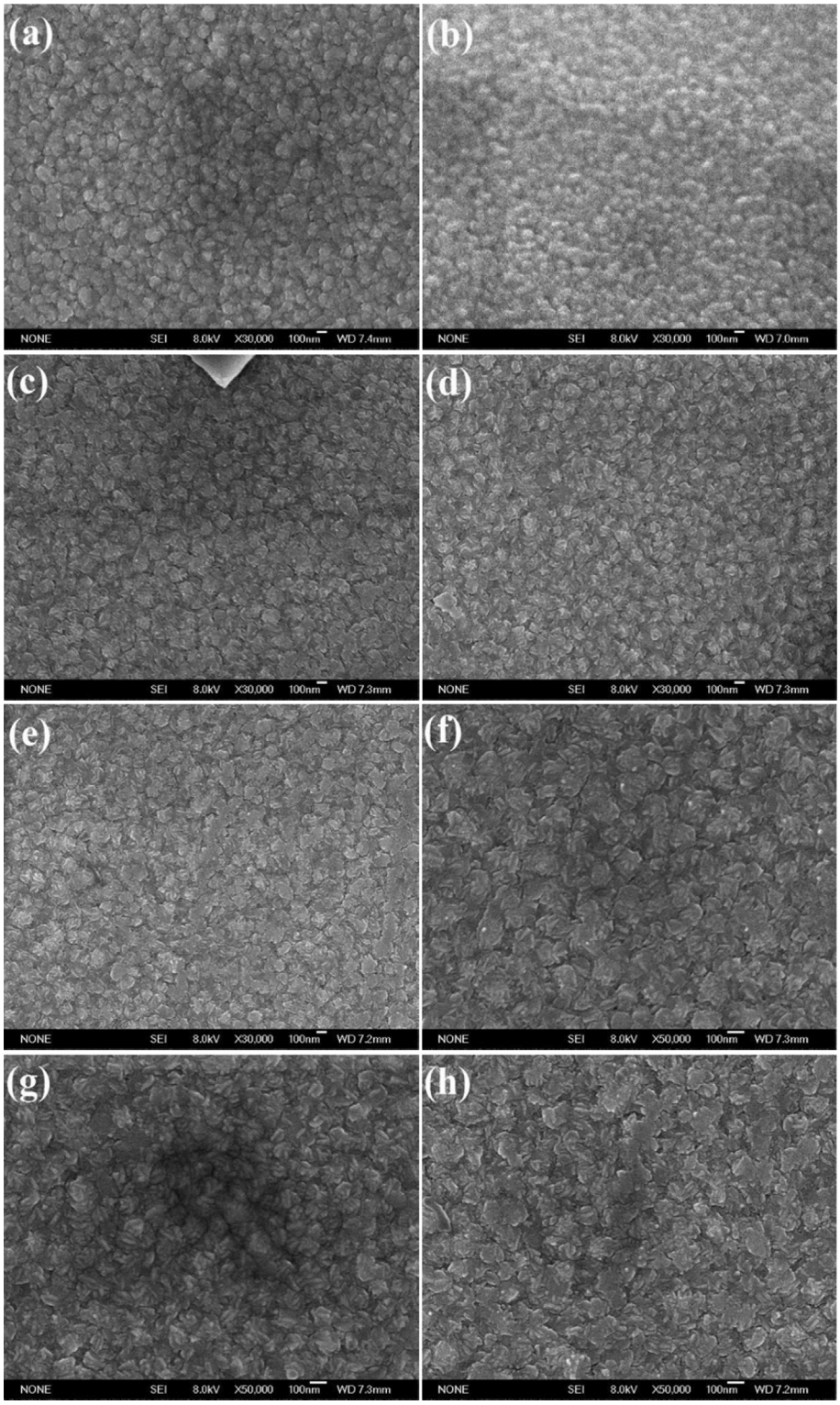

Fig. 3. Typical SEM images of the CuO_x thin films with Ar/O_2 (a) 30:5 (×30,000), (b) 30:6 (×30,000), (c) 30:7 (×30,000), (d) 30:8 (×30,000), (e) 30:9 (×30,000), (f) 30:7 (×50,000), (g) 30:8 (×50,000), (h) 30:9 (×50,000).

which are relevant to the electrochemical properties of the semiconductor materials. The corresponding results are shown in Fig. 7A–E. As shown in Fig. 7A and B, compared with these CuO_x thin film photocathodes, the impedance arc of the 30:7 CuO_x thin film photocathode increased dramatically, indicating that the 30:7 CuO_x thin film has strong semiconductor properties. In addition, the impedance arc of the 30:5 and 30:6 CuO_x thin film photocathodes are very small, it

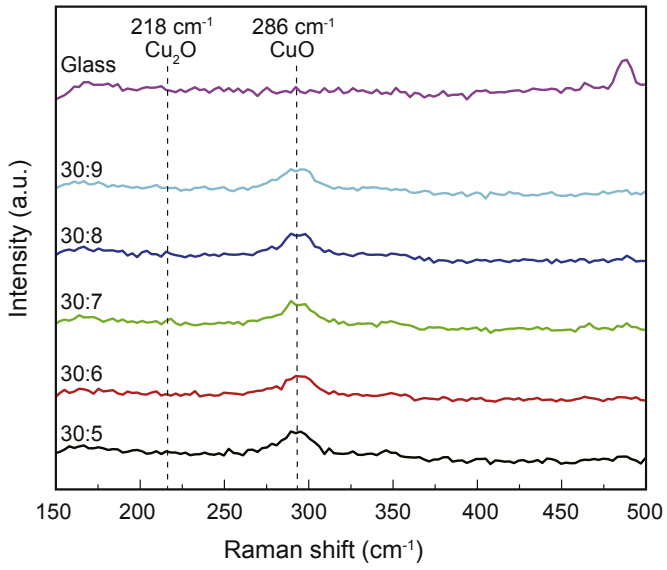

Fig. 4. Raman spectra of CuO_x composite with different Ar/O_2 ratios.

can be declared that 30:5 and 30:6 CuO_x thin films have metalloid properties, that means there is a small amount of Cu in the sputtered products of these thin films. Because of the huge change of the EIS data, different fit circuits should be employed to simulate different CuO_x thin film photocathodes. The corresponding fit circuits and fit data are shown in Fig. 7C–E, respectively. In Fig. 7C, R_{sol} is the solution resistance; R_t and C_t are the resistance and capacitance of electrons transfer in the photocathode thin films respectively; CPE_{ss} is constant phase angle element. R_{ss} was used to describe the charge transfer resistance between the semiconductor and the electrolyte interface. The fit circuits show a good simulation of the EIS curve of CuO_x thin films photocathodes as shown in Fig. 7C–E. Table 1 shows the corresponding fit data, in which two key parameters R_t and R_{ss} are 5.206×10^3 and 42.25 $\Omega\ cm^{-2}$. Fig. 7D shows the fit circuit and fit data of the CuO_x thin film at 30:6, compared with Fig. 7C, a C_{ss} was used to replace CPE_{ss}, and CPE_t was used to replace C_t. As shown in Table 1, the R_t and R_{ss} are 1.077×10^{-4} and 33.31 $\Omega\ cm^{-2}$. Fig. 7E shows the fit circuits and fit data of the CuO_x thin films at 30:7, 30:8 and 30:9. Compared with Fig. 7C, C_{ss} was used to replace CPE_{ss}, R_t and R_{ss} are shown in Table 1. Compared with these values, we can find the R_t of CuO_x thin film at 30:5 increased near 10^7 orders of magnitude than that of other CuO_x thin films. Meanwhile, the R_{ss} of CuO_x thin films at 30:7 and 30:8 increased 100 orders of magnitude than that of other thin films.

Fig. 7F shows the Mott–Schottky plots of the CuO_x thin film photoelectrodes in 0.1 M Na_2SO_4 under dark condition. According to the Mott–Schottky plots shown in Fig. 7F, both of the CuO_x thin films exhibit the characteristics of p-type semiconductors. Mott–Schottky is a mathematical equation (as shown in followed Eq. (1)), which describes the relationship between the capacitance of semiconductor space charge layer and the applied potential.

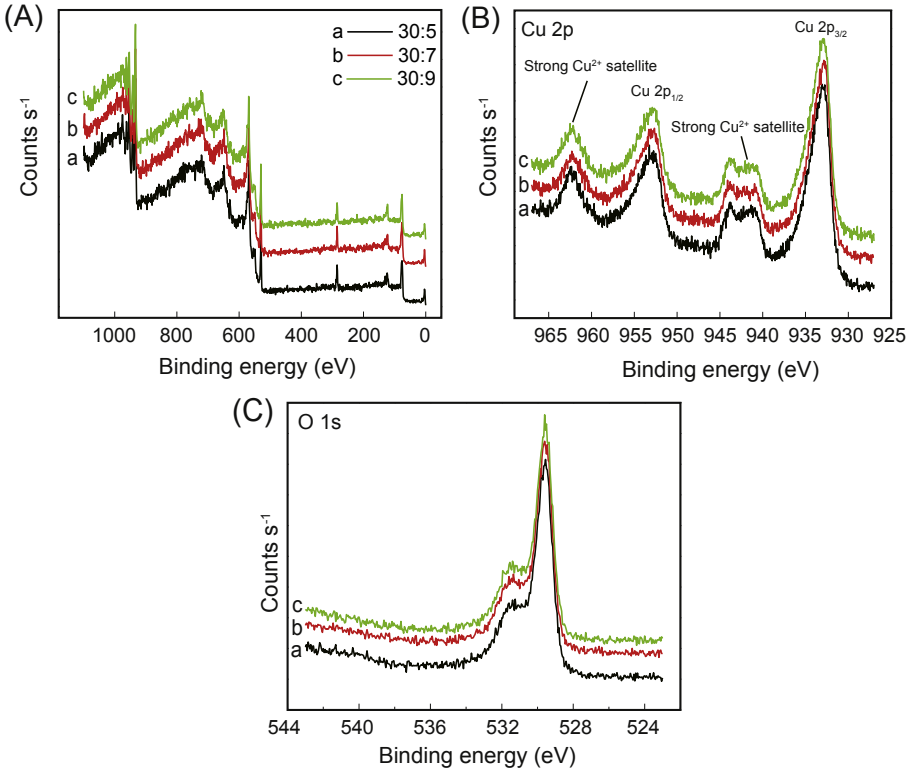

Fig. 5. XPS spectra of CuO_x composite with different Ar/O_2 ratios. (A) Wide scan result; (B) Cu 2p; (C) O 1s.

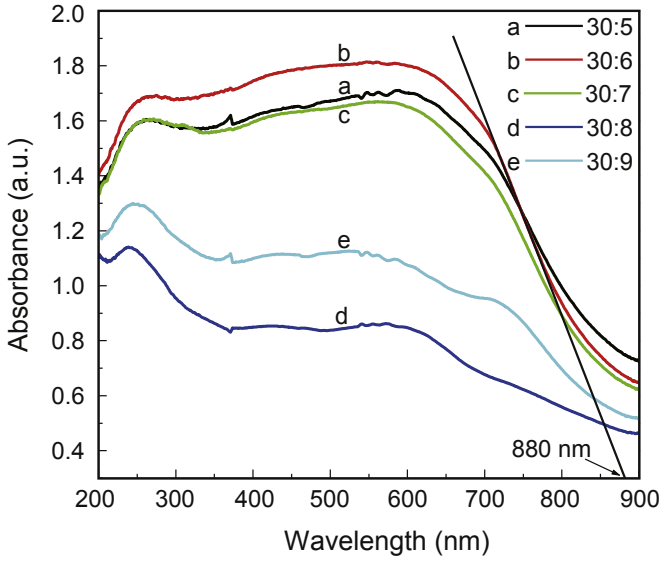

Fig. 6. UV–Vis absorption spectra of CuO_x composite with different Ar/O_2 ratios.

$$\frac{1}{C^2}=\frac{2}{\varepsilon\varepsilon_0 q N_q}\cdot\left(E-E_{fb}-\frac{kT}{q}\right) \quad (1)$$

where C is the capacitance of semiconductor space charge layer, ε is the relative permittivity of the semiconductor, ε_0 is the permittivity of vacuum (8.85×10^{-14} F cm^{-1}), q is the elemental charge (electron is +e, hole is −e, e = 1.602×10^{-19} C), N_q is the carrier concentration, E_{fb} is the flat band potential, E is the applied potential, k is the Boltzmann constant ($k = 1.38 \times 10^{-23}$ J K^{-1}), and T is the temperature. According to the negative tangent slopes in Fig. 7F, all of the CuO_x photoelectrodes exhibited the characteristics of p-type semiconductors. According to Eq. (1), $\frac{1}{C^2}$ and E is linear relation, the carrier concentration can be obtained from the tangent slope, and the flat band potential of the semiconductor material can be got by the intercept of the tangent and the potential axis. The flat band potential of the CuO_x photoelectrode at 30:5 is approximately 0.69 V (vs. Ag/AgCl), after the increasing of Ar/O_2 ratio, the flat band potentials of the CuO_x photoelectrodes are negatively shifted to 0.61, 0.64 and 0.66 V, respectively. According to Eq. (1), the negative shift of the tangent slope will increase the carrier concentration, therefore, improving the photoelectrochemical performance of the CuO_x photoelectrodes.

The photoinduced volt–ampere characteristic curve (i–V curve) of CuO_x thin film photoelectrodes are shown in Fig. 8A. Current–potential characteristics in 0.1 M Na_2SO_4 solution, under chopped AM 1.5 light illumination to study the photoelectrochemical response. The photoinduced current with potential was tested from 0.5 V to −0.5 V (vs. Ag/AgCl) with a scan rate of 0.02 V s^{-1}, and the photoinduced I–V curve was performed during light on and off in turns with 1 s respectively. The cathodic photocurrent feature of the thin films confirmed that the CuO_x is p-type, which agreed with those

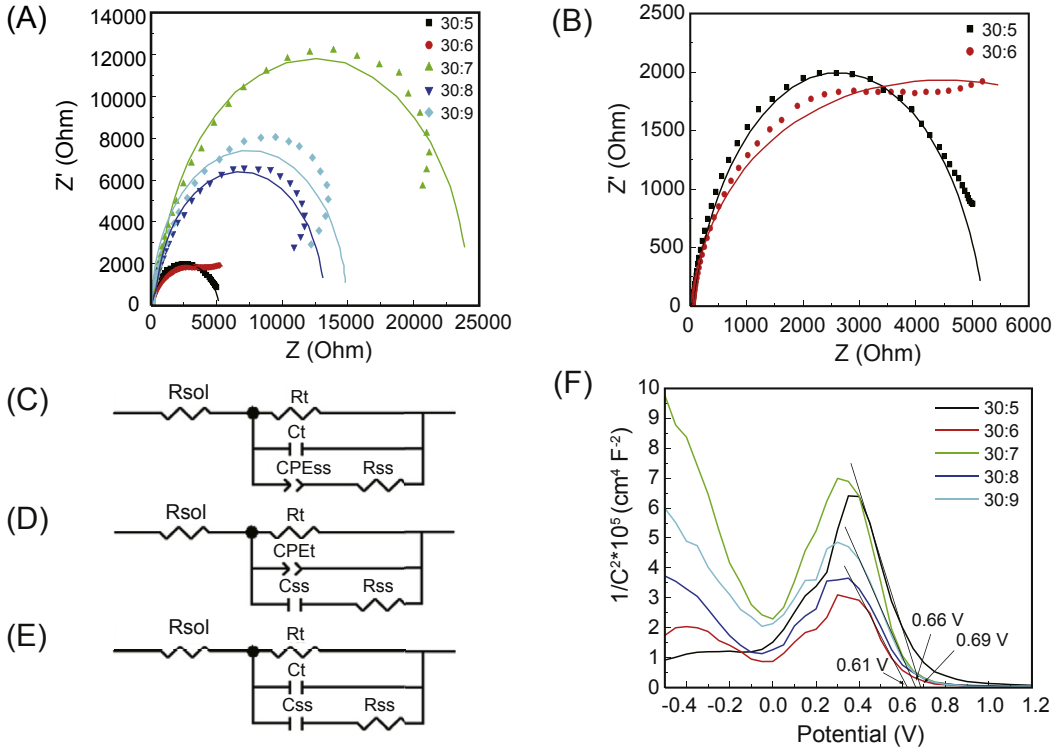

Fig. 7. (A) EIS spectra of CuO_x thin films under different Ar/O_2 ratios in 0.1 M Na_2SO_4 electrolyte. (B) Enlarged view of 30:5 and 30:6. (C) The fit circuit of 30:5 EIS curves. (D) The fit circuit of 30:6 EIS curves. (E) The fit circuit of 30:7, 30:8 and 30:9 EIS curves. (F) Mott–Schottky plots of CuO_x composite with different Ar/O_2 ratios.

Table 1
Fitted parameters of the EIS of CuO_x thin films based on the circuits shown in Fig. 7C–E.

Sample	R_{sol} [Ω cm^2]	R_t [Ω cm^2]	CPE [$Ω^{-1}$ cm^2 sn]	n	C_t [F cm^{-2}]	C_{ss} [F cm^{-2}]	R_{ss} [Ω cm^2]
30:5	1.706	5.206×10^3	1.23×10^{-5}	0.8361	7.696×10^{-8}	–	42.25
30:6	21.4	1.077×10^{-4}	1.051×10^{-4}	0.3935	–	1.004×10^{-5}	33.31
30:7	54.32	2.417×10^{-4}	–	–	4.173×10^{-6}	3.52×10^{-6}	2797
30:8	45.48	1.316×10^{-4}	–	–	5.956×10^{-6}	6.309×10^{-6}	1420
30:9	14.74	1.489×10^{-4}	–	–	8.921×10^{-9}	7.812×10^{-6}	53.1

from the results of Mott–Schottky. The photoinduced current densities of these photoelectrodes start at approximately 0.2 V and increase with the negative shift of the bias potential. The CuO_x thin film photocathode with Ar/O_2 30:7 generated a photoinduced current density of −3.2 mA cm^{-2} at the bias potential of −0.5 V vs. RHE, which was about twice that of the Ar/O_2 30:5. However, the photoinduced current densities become lower with the increase of O_2 gas flow after $Ar/O_2 = 30:7$. The results show that the most suitable Ar/O_2 ratio is 30:7 for the photoelectrochemical performance. The incident photon-to-current conversion efficiency (IPCE) results of the CuO_x with Ar/O_2 30:5, 30:7 and 30:9 were showed in Fig. 8B. The IPCE values of all samples decline rapidly since the wavelength larger than 700 nm, and terminate near 900 nm. In addition, CuO_x 30:7 photocathode shows the highest IPCE value in all photo response range, which value is near twice higher than CuO_x 30:5 and 1.5 times higher than CuO_x 30:9 photocathode respectively. The photoinduced i–t curve of the well-defined CuO_x thin film photoelectrode ($Ar:O_2 = 30:7$) is shown in Fig. 8C. The bias potential for measuring the i–t curve is 0 V. According to the i–t curve, the CuO_x with Ar/O_2 30:7 photoelectrode is stable under the bias potential of 0 V. In addition, a negative current peak appeared after turning on the light, demonstrating that there are some defects in the CuO_x photoelectrode. The formation of the strong current peak is due to an instantaneous photoelectrons charging process. Compare with the SEM images (the insets of Fig. 8C) of the CuO_x photoelectrode before and after i–t test, the morphologies of the CuO_x have some varieties, indicating that CuO_x has a certain degree of corrosion in the process of i–t measurement. Therefore, we decided to make a protective layer coating on the surface of the CuO_x to protect it from corrosion in the future.

Fig. 9 shows the mechanism of the CuO_x thin film grown on the FTO substrate. Under light illumination, the photovoltaic effect of CuO_x semiconductor material resulted in the generation of electrons and holes. With the extra applied negative bias potential, the conduction band potential of CuO_x will be more negative than that of water reduction potential, the photogenerated electrons with strong reduction capacity can

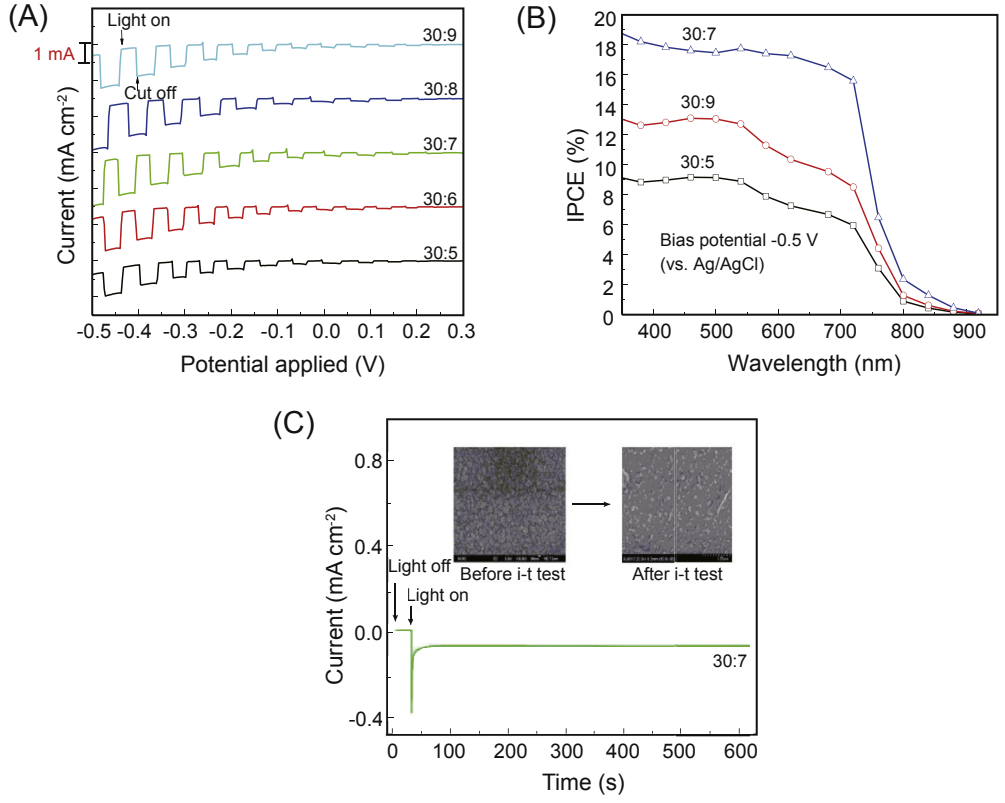

Fig. 8. (A) The photoinduced volt-ampere characteristic curve (i–V curve), (B) the incident photon-to-current conversion efficiency (IPCE) results, (C) the photoinduced i–t curve (the insets show the SEM images of the CuO_x thin film photoelectrode before and after i–t test) of the CuO_x thin film photoelectrode.

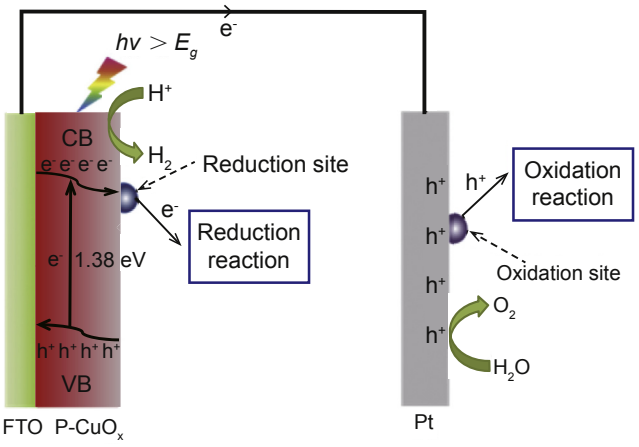

Fig. 9. Schematic illustration of the mechanism of the CuO_x thin film photocathode.

shift to the surface of CuO_x thin film and reduce water to hydrogen. The photogenerated holes will transfer to the FTO substrate. On the other hand, the photogenerated electrons from Pt counter will also transfer to the CuO_x photocathode, meanwhile, the photogenerated holes will shift to the surface of Pt counter, and finally oxidize water to oxygen.

4. Conclusions

In summary, the CuO_x thin films with different Ar/O_2 gas ratios were successfully prepared by magnetron reactive sputtering on the FTO glasses. The deposited products have been demonstrated to be mixtures of Cu_2O and CuO, and the content of CuO is higher than Cu_2O synthesized in these thin films. Compared with different Ar/O_2 gas ratios, the well-defined CuO_x thin films with Ar/O_2 ratio 30:7, are demonstrated to display much better photoelectrochemical performance. Subsequently, UV/Vis diffuse reflectance spectroscopy, EIS, Mott–Schottky tests were carried out. It was found that the CuO_x thin films under lower O_2 gas flows (Ar/O_2 = 30:5, 6, 7) have strong light absorption capability in ultraviolet and visible light region. The CuO_x thin film under the gas ratio of 30:7 has the biggest impedance value and fewer defects, indicating that the CuO_x thin film under the gas ratio of 30:7 has strong semiconductor properties.

Conflict of interest

There is no conflict of interest.

Acknowledgements

This work was financially supported by the National Natural Science Foundation of China (Grant Nos. 41506093).

References

[1] J. Cen, Q. Wu, M. Liu, A. Orlov, Green Energy Environ. 2 (2017) 100–111.
[2] S.K. Mohapatra, S.E. John, S. Banerjee, M. Misra, Chem. Mater. 21 (2009) 3048–3055.
[3] S.W. Boettcher, J.M. Spurgeon, M.C. Putnam, E.L. Warren, D.B. Turner-Evans, M.D. Kelzenberg, J.R. Maiolo, H.A. Atwater, N.S. Lewis, Science 327 (2010) 185–187.
[4] Y. Lin, S. Zhou, S.W. Sheehan, D. Wang, J. Am. Chem. Soc. 133 (2011) 2398–2401.
[5] Y. Lin, G. Yuan, S. Sheehan, S. Zhou, D. Wang, Energy Environ. Sci. 4 (2011) 4862–4869.
[6] B. Klahr, S. Gimenez, F. Fabregat-Santiago, J. Bisquert, T.W. Hamann, J. Am. Chem. Soc. 134 (2012) 16693–16700.
[7] B. Seger, A.B. Laursen, P.C.K. Vesborg, T. Pedersen, O. Hansen, S. Dahl, I. Chorkendorff, Angew. Chem. Int. Ed. 51 (2012) 9128–9131.
[8] Y.W. Chen, J.D. Prange, S. Dühnen, Y. Park, M. Gunji, C.E.D. Chidsey, P.C. Mclntyre, Nat. Mater. 10 (2011) 539–544.
[9] Y. Bu, J.P. Ao, Green Energy Environ. 2 (2017) 331–362.
[10] F. Le Formal, N. Tétreault, M. Cornuz, T. Moehl, M. Grätzel, K. Sivula, Chem. Sci. 2 (2011) 737–743.
[11] M. Barroso, A.J. Cowan, S.R. Pendlebury, M. Grätzel, D.R. Klug, J.R. Durrant, J. Am. Chem. Soc. 133 (2011) 14868–14871.
[12] Y.F. Lim, C.S. Chua, C.J.J. Lee, D. Chi, Phys. Chem. Chem. Phys. 16 (2014) 25928–25934.
[13] Y. Yang, D. Xu, Q. Wu, P. Diao, Sci. Rep. 6 (2016) 35158.
[14] C. Li, T. Hisatomi, O. Watanabe, M. Nakabayashi, N. Shibata, K. Domen, J.J. Delaunay, Energy Environ. Sci. 8 (2015) 1493–1500.
[15] A. Paracchino, V. Laporte, K. Sivula, M. Grätzel, E. Thimsen, Nat. Mater. 10 (2011) 456–461.
[16] G. Liu, S. Ye, P. Yan, F. Xiong, P. Fu, Z. Wang, Z. Chen, J. Shi, C. Li, Energy Environ. Sci. 9 (2016) 1327–1334.
[17] T.W. Kim, K.S. Choi, Science 343 (2014) 990–994.
[18] Y.H. Ng, A. Iwase, A. Kudo, R. Amal, J. Phys. Chem. Lett. 1 (2010) 2607–2612.
[19] M. Higashi, R. Abe, T. Takata, K. Domen, Chem. Mater. 21 (2009) 1543–1549.
[20] V. Cristino, S. Caramori, R. Argazzi, L. Meda, G.L. Marra, C.A. Bignozzi, Langmuir 27 (2011) 7276–7284.
[21] A. Kay, I. Cesar, M. Grätzel, J. Am. Chem. Soc. 128 (2006) 15714–15721.
[22] K. Sivula, F. Le Formal, M. Grätzel, ChemSusChem 4 (2011) 432–449.
[23] A.A. Dobale, A.G. Tamirat, H.M. Chen, T.A. Berhe, C.J. Pan, W.N. Su, B.J. Hwang, J. Mater. Chem. A 4 (2016) 2205–2216.
[24] Q. Huang, F. Kang, H. Liu, Q. Li, X. Xiao, J. Mater. Chem. A 1 (2013) 2418–2425.
[25] Z. Zhang, P. Wang, J. Mater. Chem. 22 (2012) 2456–2464.
[26] K. Nakaoka, J. Ueyama, K. Ogura, J. Electrochem. Soc. 151 (2004) C661–C665.
[27] N. Mukherjee, B. Show, S.K. Maji, U. Madhu, S.K. Bhar, B.C. Mitra, G.G. Khan, A. Mondal, Mater. Lett. 65 (2011) 3248–3250.
[28] Y. Bessekhouad, D. Robert, J.-V. Weber, Catal. Today 101 (2005) 315–321.
[29] S. Masudy-Panah, R.S. Moakhar, C.S. Chua, H.R. Tan, T.I. Wong, D. Chi, G.K. Dalapati, ACS Appl. Mater. Interfaces 8 (2016) 1206–1213.
[30] G. Malandrino, S.T. Finocchiaro, R.L. Nigro, C. Bongiorno, C. Spinella, Chem. Mater. 16 (2004) 5559–5561.
[31] Y. Yang, Y. Li, M. Pritzker, Electrochim. Acta 213 (2016) 225–235.
[32] G.K. Dalapati, S. Masudy-Panah, A. Kumar, C.C. Tan, H.R. Tan, D. Chi, Sci. Rep. 5 (2015) 17810.